Progress In Electromagnetics Research, Vol. 151, 55–63, 2015

Meander-Line Based Broadband Artificial Material for Enhancing the Gain of Printed End-Fire Antenna

Lei Chen*, Zhenya Lei, and Xiaowei Shi

Abstract—A broadband artificial material based on meander-line (ML) structures is proposed for enhancing the gain of printed end-fire antennas. The ML based material with an effective index of refraction greater than 1 behaves as a dielectric lens in improving the directivity of an end-fire antenna. The electric field intensity distribution can be changed by the material, resulting in a more directional emission. Simulated results indicate extending the length or width of the material can lead to more significant gain enhancement without destroying the impedance bandwidth of the antenna. Three printed end-fire antennas with and without material loading are fabricated and measured. The measurements show that end-fire antennas loaded with two and four rows of ML structures can obtain gain increments of 0.6–3.6 dB and 1.2–5.7 dB, respectively, and that the radiation patterns are narrowed in both E- and H-planes over the whole operating band (6–11.5 GHz).

1. INTRODUCTION

Over the past decade, artificial materials or metamaterials typically consisting of an array of electrically small particles have been extensively investigated. As the controllable electromagnetic response of the material elements, artificial materials can present negative, near-zero, or positive refractive index. These materials with anomalous electromagnetic properties have been widely applied to the design of metamaterial devices to obtain improved performance or unconventional properties [1, 2]. Many of the recent advances in metamaterials have been focused on the design of a variety of meta-based antennas [3, 4].

Recently, various metamaterial lenses have been designed to improve the directivity of the traditional antennas. Made by graded photonic crystal, the gradient-index lens can lead to high gain and low sidelobes with this lens placed inside a horn antenna [5]. Using gradient-index or zero-index metamaterials, three-dimensional anisotropic lenses have been designed and experimentally demonstrated in [6, 7]. Composed of conventional and epsilon near-zero materials, a flat lens has been proposed to shorten the length of a horn antenna without decreasing its directivity in a broad frequency range [8]. Moreover, the electromagnetic bandgap (EBG) structures as a superstrate can filter the undesired radiation for a class of patch antennas [9].

Printed end-fire antennas have been extensively investigated as their low cost, low profile, and ease of fabrication. To improve the radiation performance of printed end-fire antennas, artificial materials have also been widely exploited due to their significant enhancement ability in directivity. The inherent characteristics of material elements determine the gain enhancement ability or bandwidth of the material. By loading a zero-index metamaterial with one component of the effective permittivity approaching zero, tapered slot antennas can achieve a high gain within the expected narrow frequency band [10, 11]. While employing parallel-line structures, the tapered slot antenna can realize gain enhancement in broadband [12]. The resonant structures such as the split-ring resonators or I-shaped resonators have also been used to improve the radiation performance of periodic end-fire

Received 14 February 2015, Accepted 3 April 2015, Scheduled 13 April 2015
* Corresponding author: Lei Chen (1225chenlei@163.com).
The authors are with the School of Electronic Engineering, Xidian University, Xi'an 710071, China.

antennas [13, 14]. Moreover, loaded with H-shaped resonators, a broadband vertical planar antenna with enhanced gain over 2.31–3.93 GHz is proposed in [15].

Artificial materials constructed by non-resonant elements may present a large frequency bandwidth [16]. For the purpose of enhancing the gain of a printed end-fire antenna with broad bandwidth, we propose the non-resonant meander-line (ML) based artificial material and place it in front of the antenna.

The structure of the paper is as follows. In Section 2, the effective parameters of the proposed material are retrieved, the reasons for gain improvement by the proposed material are investigated, and for an end-fire antenna, the enhanced gain by a dielectric lens and the ML-based material are compared. After that, we demonstrate the gain enhancement effect of the material with respect to its dimensions. In Section 3, results from simulations and measurements for end-fire antennas with and without material loading are compared and discussed in detail. In Section 4, the main work is summarized.

2. MEANDER-LINE BASED MATERIAL FOR GAIN ENHANCEMENT

ML structures have been used as the constitutive elements of a negative index material in [17]. We here utilize the non-resonant characteristic of the ML structure. The geometry of the ML structure and the simulation model in High Frequency Structure Simulator (HFSS) are demonstrated in Fig. 1(a). Dimensions of the ML structure are $a = 7\,\text{mm}$, $m_x = 4.8\,\text{mm}$, $m_y = 5.1\,\text{mm}$, $w = 0.2\,\text{mm}$, and $t = 1\,\text{mm}$. The substrate is chosen as F4B with the permittivity (ε_r) of 2.2 and the tangent loss of 0.001. The electrical polarization of the simulation model is along the x-axis. As shown in Fig. 1(a), the perfect electric conductor (PEC) boundaries are set on the up-down faces (yz-planes) of the box and the perfect magnetic conductor (PMC) boundaries on the front-back faces (xy-planes).

All simulations are performed by the full-wave simulation software HFSS. In Fig. 2(a), the simulated scattering parameters of the ML based material are presented, showing that the magnitude of reflection coefficient (S_{11}) of the material is well below $-10\,\text{dB}$ from 5 GHz to 11.5 GHz. Thus, within this frequency band electromagnetic waves can transmit through the material with low return loss. For qualitative analysis, the electromagnetic properties of the material are approximately described in terms of effective parameters, as the elements are electrically small in low frequency band. As shown in Fig. 2(b), the effective index of refraction (n), retrieved by a standard procedure [19], varies in the range of 1.34–1.47 in the non-resonant region (5–11.5 GHz). Fig. 2(c) presents the normalized impedance of the material, the real value of which is near unity within the non-resonant region, ensuring a good match between the antenna and air. The extracted effective permittivity and permeability are demonstrated in Fig. 2(d), where the permittivity is greater than unity.

To verify the gain enhancement effect of the proposed material, we select the periodic end-fire antenna (PEF) as the printed end-fire antenna for its stable gain in a wide frequency band. Proposed in [18], the PEF antenna is composed of three different-sized bowtie dipoles connected to a parallel strip line, and fed by a microstrip line. The artificial material loaded PEF antenna, as shown in Fig. 1(b), has

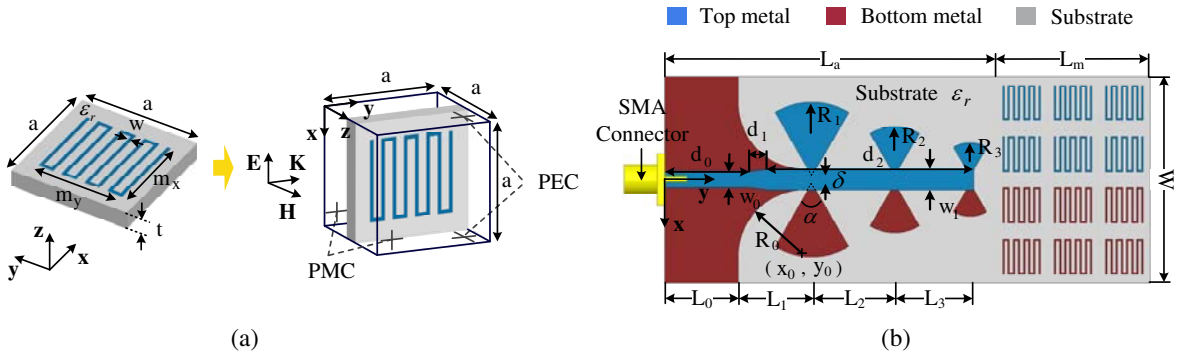

Figure 1. (a) The geometry and simulation model of the ML structure cell. (b) The PEF antenna loaded with three rows of proposed ML based artificial material.

the dimensions: $W = 28\,\text{mm}$, $L_a = 45\,\text{mm}$, $L_m = 21\,\text{mm}$, $L_0 = 10\,\text{mm}$, $L_1 = 10\,\text{mm}$, $L_2 = 11.25\,\text{mm}$, $L_3 = 10.25\,\text{mm}$, $R_0 = 9\,\text{mm}$, $R_1 = 10\,\text{mm}$, $d_0 = 11.4\,\text{mm}$, $d_1 = 2.6\,\text{mm}$, $d_2 = 28\,\text{mm}$, $w_0 = 2.1\,\text{mm}$, $w_1 = 2.8\,\text{mm}$, and $\delta = 1\,\text{mm}$. The radii of the three bowtie-shaped elements are R_1, R_2, and R_3, with the relationship of $R_2/R_1 = R_3/R_2 = v$ ($v = 0.67$). Two symmetrical curves in bottom layer are two quarter-circles with radius R_0, one center of which is at the position of ($x_0 = 10.4$, $y_0 = 19$) mm. The flare angles of the bowtie-shaped structures are $\alpha = 60°$. The substrate is identical with that in Fig. 1(a). The artificial material consists of 4 by 3 ML structures.

To illustrate the gain enhancement effect the ML based material, we make a comparison of the realized gain of the PEF antenna loaded with four types of materials as shown in Fig. 3(a). The refractive indexes of Material 2 and Material 4 are set as 1.47 and 1.34 respectively, which are the maximum and minimum values of the effective refractive index of the proposed material in the non-resonant region. Comparisons of the realized gain are reported in Fig. 3(b). It shows that the antenna loaded with Material 1 presents a small increase of gain compared with the unloaded one, while obvious enhancement of gain is observed for the antennas loaded with Material 2, 3 and 4. The increased gain produced by Material 2 and 3 are greater than that by Material 4 over the whole operating band (6–11.5 GHz). Thus, the ML-based material acts as a dielectric lens in gain enhancement within the operating band of the antenna. However, the advantage of Material 3 over Material 2 and 4 is that it

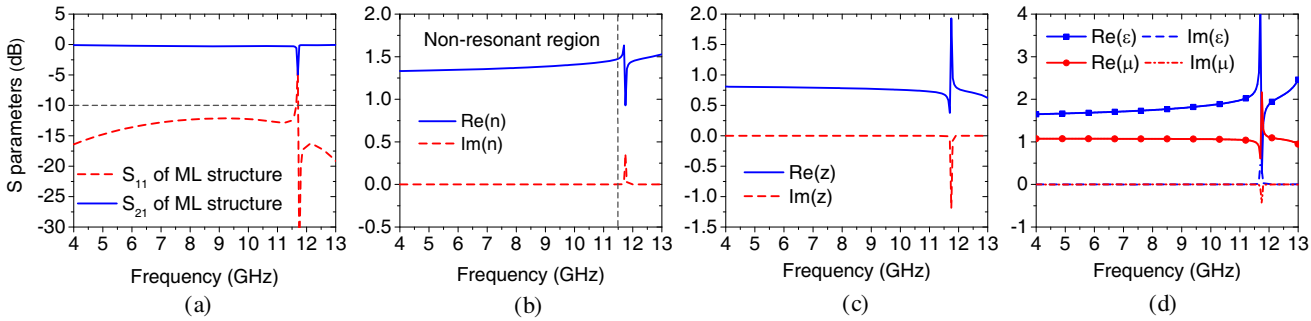

Figure 2. (a) The simulated scattering parameters of the ML based material. (b) The retrieved refractive index of the material. The left region of the dished line is the non-resonant region. (c) The normalized impedance. (d) The extracted effective permittivity and permeability.

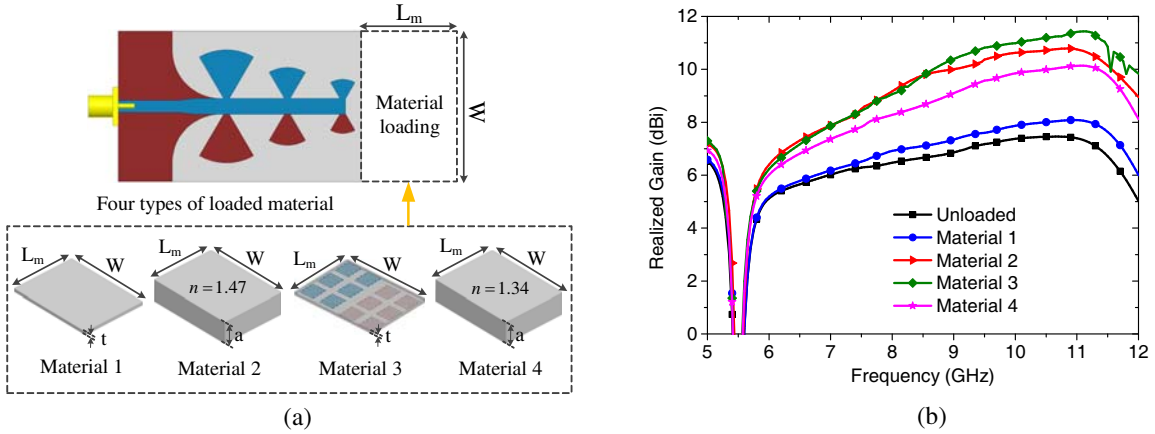

Figure 3. (a) The unloaded PEF antenna and the ones loaded with four types of materials including an extended substrate without ML structures (Material 1), two dielectric lenses with the thickness of a and with the refractive indexes of 1.47 (Material 2) and 1.34 (Material 4), and the proposed artificial material with three rows of ML structures (Material 3). (b) Comparisons of the simulated realized gain of the unloaded PEF antenna and the ones loaded with the four types of materials in Fig. 3(a).

can be integrated with the host antenna smoothly without increasing the whole thickness, which brings much more convenience for practical applications.

Figure 4(a) shows the sketch map of electromagnetic waves transmitting from the ML based material to air in xy- and yz-planes. The propagation of electromagnetic waves in artificial materials follows Snell's law $n \cdot \sin(\theta) = n_0 \cdot \sin(\theta_0)$. When the refractive index of the material (n) is greater than that of air (n_0), electromagnetic waves transmitting through the material will be converged. In the non-resonant region, the retrieved refractive index of the loaded material is greater than 1 (see Fig. 2(b)). Thus, the phase velocity in artificial material will be lower than that in air, which will compensate the phase shift produced by different materials, resulting in more planer phase fronts. It can be predicted that the radiation patterns of the proposed PEF antenna will be narrowed in both E- and H-planes. Furthermore, the electric field distributions of the PEF antennas with and without artificial materials in xy-plane are demonstrated in Figs. 4(b) and 4(c). We find that the ML based material does affect the distribution of the near field, and that the material loaded antenna obtains a larger field intensity than the unloaded one.

As demonstrated in Fig. 5(a), PEF antennas loaded with different-sized materials are designed. The simulated results, including the realized gain and the magnitudes of S_{11}, are reported in Fig. 6. Fig. 6(a) shows that increasing the number of rows or columns of ML structures results in more gain increment. For the cases of loading with wider materials (Material E and F), the enhancement is more significant in the low frequency band, while for the cases of loading with Material D and F, the gain

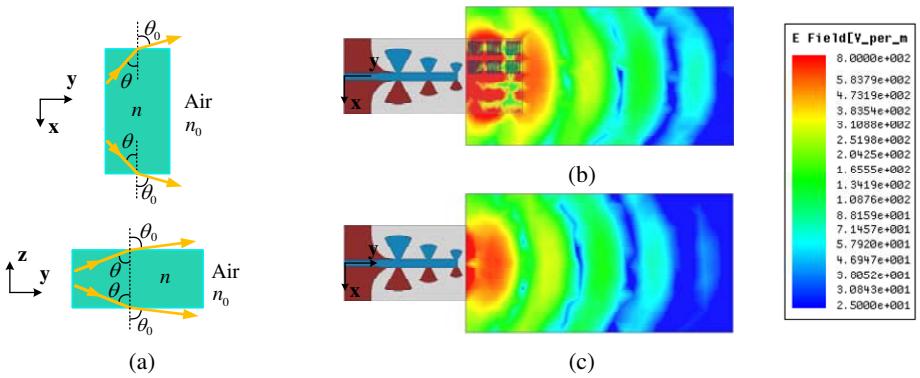

Figure 4. (a) The sketch map of electromagnetic waves transmitting through the ML based material in xy- and yz-planes. The electric field distributions of (b) the PEF antenna loaded with ML based material and (c) the unloaded PEF antenna.

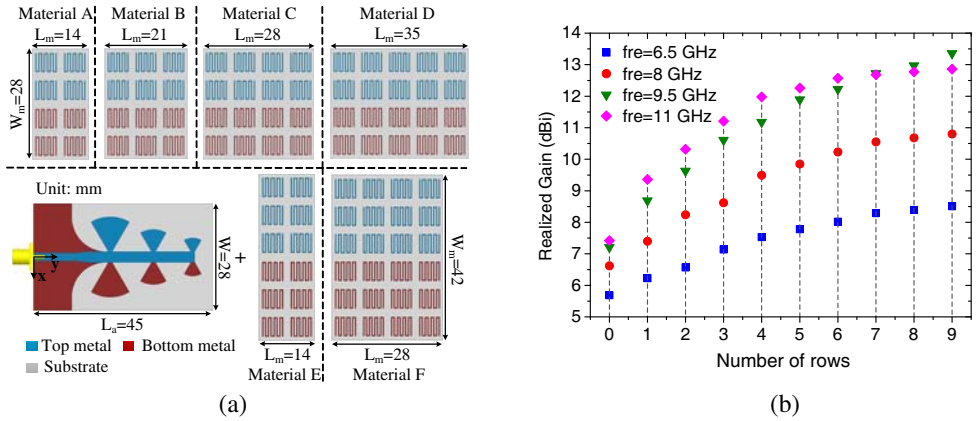

Figure 5. (a) PEF antennas loaded with the different-sized ML based materials. (b) The simulated realized gain values versus the number of rows of ML structures at the frequency of 6.5, 8, 9.5, and 11 GHz.

curves of the two PEF antennas are close in most frequency band. For all cases, nevertheless, magnitudes of S_{11} in Fig. 6(b) are less than -10 dB in the whole operating frequency band (6–11.5 GHz), which indicates the existing of the ML based material does not affect the impedance bandwidth of the PEF antennas. As the width of the material is identical with that of the antenna substrate, the gain can be enhanced further by increasing the row number of ML structures, as shown in Fig. 5(b). However, increasing the row number will result in the increase of length accordingly, and as the row number is greater than 5, the enhancement effect of the material becomes less obvious compared with Material D. Thus, for the cases of requiring high gain and miniaturization, Material B is more appropriate than other materials, taken into consideration of gain increment and antenna dimensions, while for the cases of requiring a high gain but no strictly restriction for dimensions, Material D is more appropriate than other materials.

The PEF antennas loaded with two rows of split-ring resonators (SRR) or I-shaped resonators (ISR) for gain enhancement have been proposed in [13, 14]. The models of ML structure, SRR and ISR with different electric sizes are demonstrated in Fig. 7(a). Their indexes of refraction are presented in Fig. 7(b), where the ML structure shows a stable non-resonant electromagnetic property over a broader frequency range. The characteristics of the constitutive elements will determine the material properties. A comparison of the realized gain are given in Fig. 7(c) for PEF antennas loaded with 5 rows of ML structures, SRR, and ISR, showing that the gain of the PEF antenna loaded with ML based material can also be enhanced in the high frequency band. Thus, the proposed material performs better in wideband applications than SRR and ISR based materials for gain enhancement.

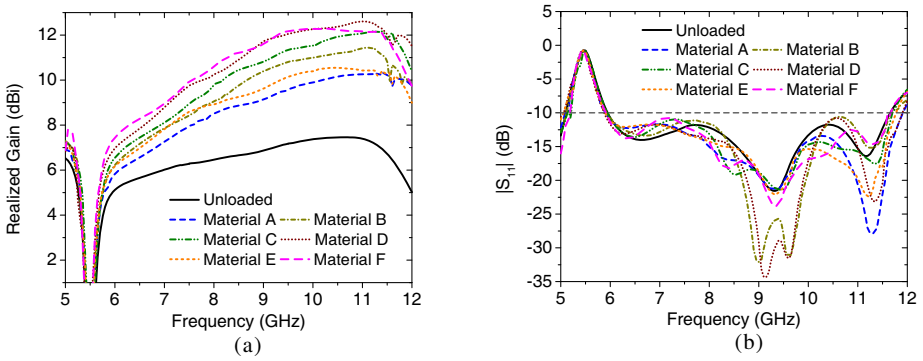

Figure 6. Comparisons of simulated (a) realized gain and (b) magnitude of reflection coefficient (S_{11}) of the unloaded PEF antenna and the ones with six types of loading cases in Fig. 5(a).

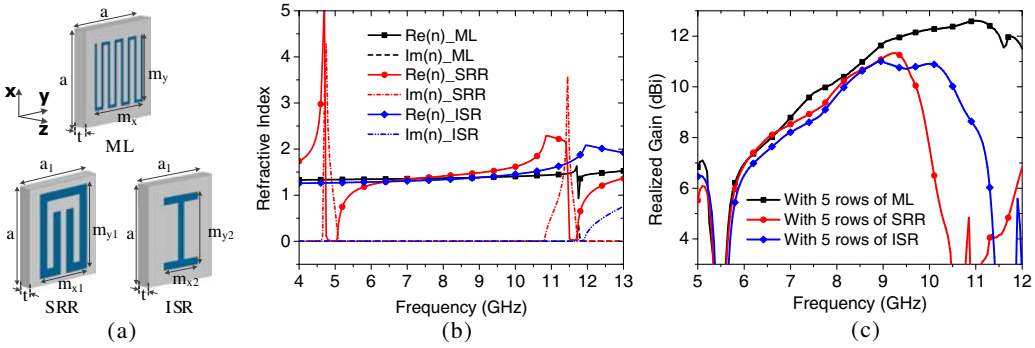

Figure 7. (a) The models of ML structure and the existing split-ring resonator (SRR) and I-shaped resonator (ISR) with the dimensions of $a_1 = 5.75$ mm, $m_{x1} = 4$ mm, $m_{y1} = 6$ mm, $m_{x2} = 3$ mm, and $m_{y2} = 5$ mm. (b) Simulated indexes of refraction of ML, SRR and ISR structures. (c) Comparisons of simulated realized gain of PEF antennas loaded with 5 rows of ML, SRR and ISR structures.

3. EXPERIMENTAL VALIDATION AND DISCUSSIONS

In this section, to validate our design, two loading cases (with Material A and C) in Fig. 5(a) are chosen for fabrication and measurement. Photographs of the fabricated antennas are shown in Fig. 8, where Antenna 1 is as reference. To verify the gain enhancement effect of the proposed materials, Antenna 4 has also been designed, which is characterized by having the same dimensions with Antenna 3, but having no ML structures on the substrate. Fig. 9(a) shows the measured and simulated gain curves of the unloaded PEF antenna (Antenna 1), the ones loaded with Material A (Antenna 2) and Material C (Antenna 3) as well as Antenna 4. It is obvious that, within the operating band, the measured gain values agree with the simulated ones for the three antennas in Fig. 8, and that Antenna 3 presents a higher gain than Antenna 4. The measured gain of Antenna 1 varies from 5.4 dBi to 6.4 dBi when

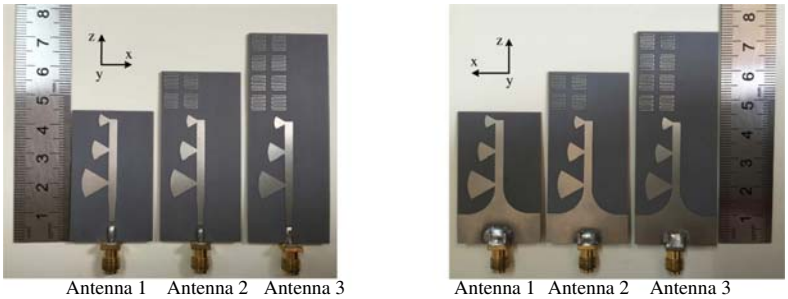

Figure 8. Photographs of unloaded PEF antenna (Antenna 1) and the ones loaded with Material A (Antenna 2) and Material C (Antenna 3). (a) The top view and (b) the bottom view of the three antennas.

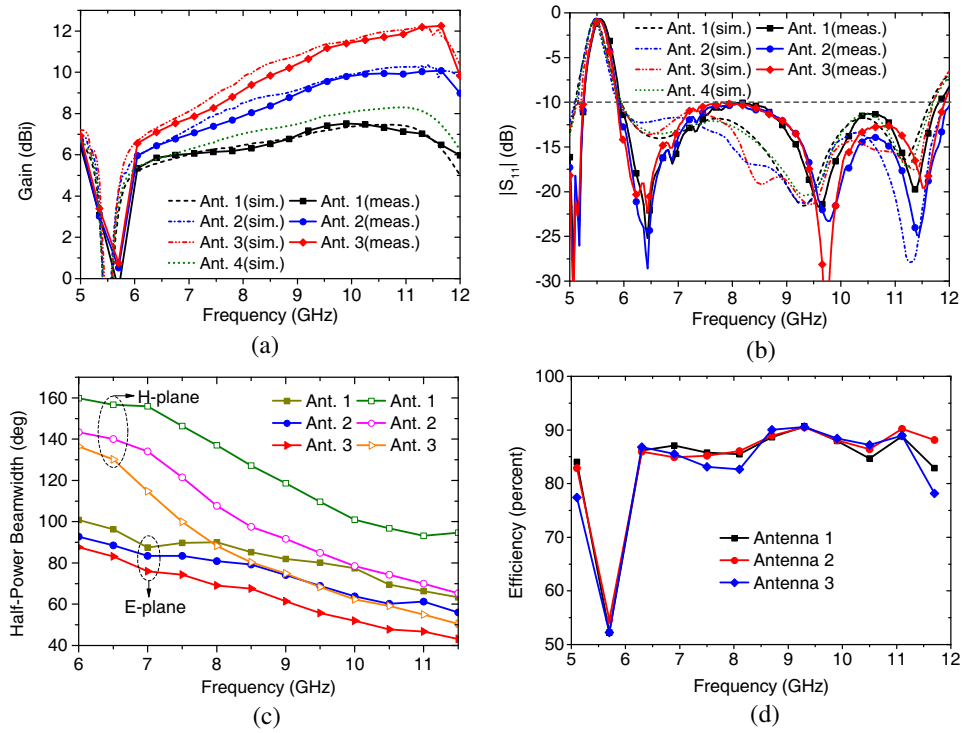

Figure 9. Comparisons of (a) gain and (b) magnitudes of S_{11} from measurements and simulations for the PEF antennas in Fig. 8 as well as Antenna 4. (c) Measured half-power beamwidths of the PEF antennas in Fig. 8 in E- and H-planes. (d) Efficiencies of the three PEF antennas.

the frequency covers 6–11.5 GHz, while Antenna 2 from 5.8 dBi to 8.4 dBi, and Antenna 3 from 6.5 dBi to 11.5 dBi. Compared with Antenna 1, Antenna 2 and 3 obtain a gain increment of 0.6–3.6 dB and 1.2–5.7 dB, respectively. Obviously, Antenna 3 obtains the highest gain among the three antennas. Furthermore, it can be seen that the high frequency band obtains more significant gain enhancement than the low frequency band. Similar conclusions can also be achieved from simulated results. It should be noted that with the increase of gain, the dimension of the loaded antenna in length has also been increased accordingly. Compared with the unloaded PEF antenna (Antenna 1), the length of Antenna 2 and 3 has been increased by 31% and 62%, respectively.

The reflection coefficients S_{11} at the input ports of the three antennas in Fig. 8 are measured using a network analyzer with the measured results given in Fig. 9(b), where the simulated S_{11} is included for comparison. It shows that the measured and simulated impedance bandwidth for magnitudes of S_{11} less than -10 dB covers 6–11.5 GHz (a percentage bandwidth of 63%) for the three antennas, indicating that the PEF antennas loaded with the ML based material match well with air. The only burden brought by this loading is that the length of the antennas is extended.

To demonstrate the beam focusing effect caused by the proposed material, Fig. 9(c) presents the half-power beamwidths in both E- and H-planes as a function of frequency for the fabricated antennas.

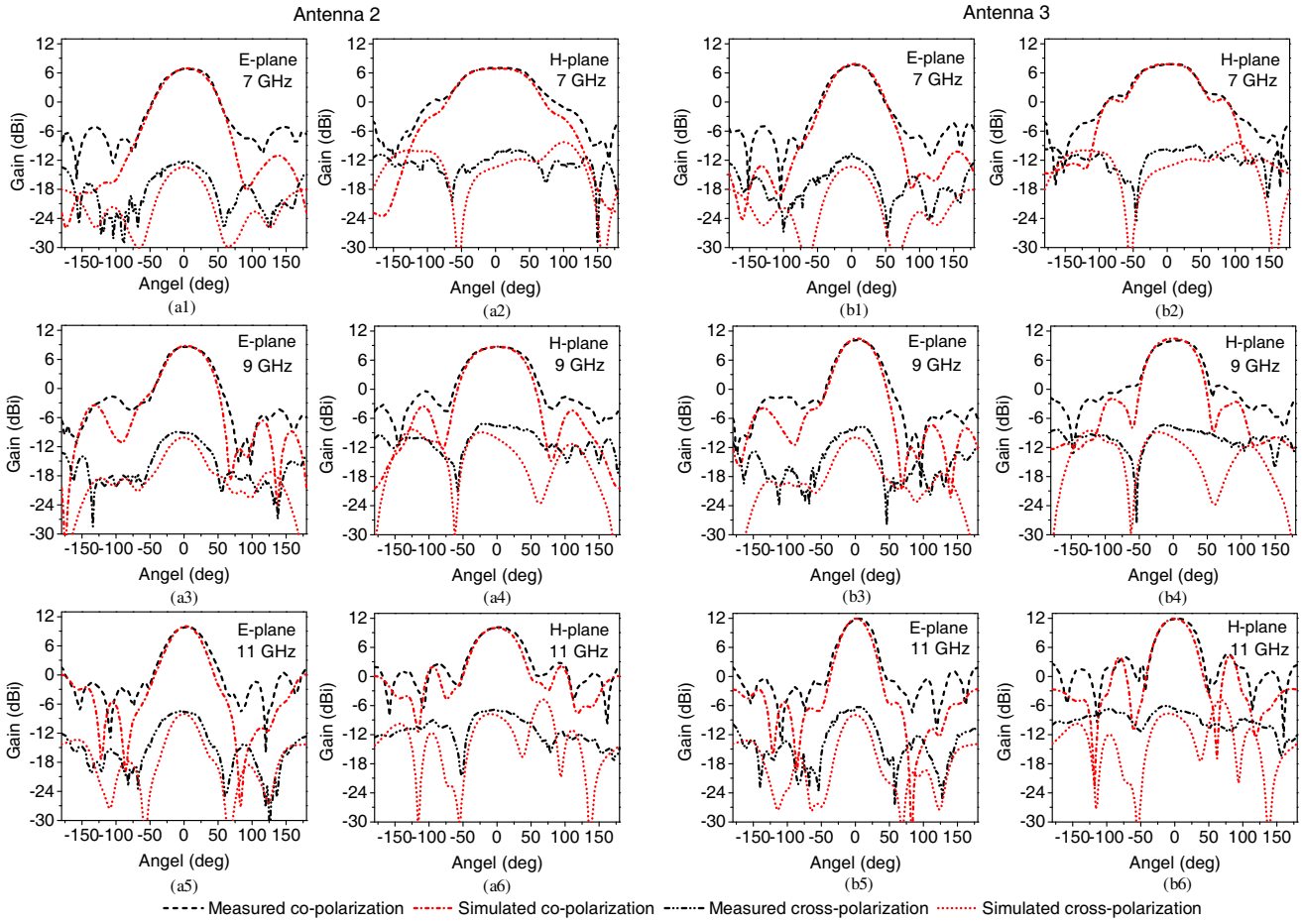

Figure 10. Measured and simulated co-polarization and cross-polarization patterns of Antenna 2 and 3 in Fig. 8. (a1) E-plane and (a2) H-plane radiation patterns of Antenna 2 at 7 GHz. (a3) E-plane and (a4) H-plane radiation patterns of Antenna 2 at 9 GHz. (a5) E-plane and (a6) H-plane radiation patterns of Antenna 2 at 11 GHz. (b1) E-plane and (b2) H-plane radiation patterns of Antenna 3 at 7 GHz. (b3) E-plane and (b4) H-plane radiation patterns of Antenna 3 at 9 GHz. (b5) E-plane and (b6) H-plane radiation patterns of Antenna 3 at 11 GHz.

In Fig. 9(c), compared with Antenna 1, the beamwidth decrement of Antenna 2 varies in the range of $4.1° - 13.6°$ and $16.5° - 29.6°$ for E- and H-planes, respectively, while Antenna 3 in the range of 11.6°–25.4° and 23.3°–48.7°. Clearly, Antenna 3 obtains a narrower beamwidth, meanwhile H-planes achieve much more beamwidth decrement than E-planes for the loaded antennas. Taken into consideration of return losses and radiation losses, efficiencies of the three antennas are more than 80% over the whole operating band as shown in Fig. 9(d), which indicates the existing of the ML based material does not lead to much more losses. In Fig. 10, we report the co-polarization and cross-polarization patterns of Antenna 2 and Antenna 3 in both E- and H-planes at three selected frequencies (7, 9 and 11 GHz). It is not hard to see that the measured main beam patterns of co-polarization agree with the simulated ones, and that the cross polarization is near 20 dB lower than co-polarization in both planes. The discrepancy between measured and simulated patterns could be caused by the misalignment of the antennas during the measurement.

4. CONCLUSION

In this paper, we have presented a broadband artificial material composed of ML structures, and applied it to gain enhancement of a printed end-fire antenna. By locating the material in front of the PEF antenna, the material can act as a thick dielectric lens in gain enhancement, and a more directional emission can be obtained. The material can be integrated with the PEF antenna smoothly, and increasing the dimensions of length or width of the material can lead to more significant gain enhancement. The measurement results agree with the simulated ones over the operating frequency band for the fabricated antennas. In addition, the broadband artificial material can also be used for radiation improvement of other types of printed end-fire antennas.

REFERENCES

1. Silveirinha, M. and N. Engheta, "Design of matched zero-index metamaterials using nonmagnetic inclusions in epsilon-near-zero media," *Physics Rev. B*, Vol. 75, No. 7, 075119, 2007.
2. Liu, R., A. Degiron, J. J. Mock, and D. R. Smith, "Negative index material composed of electric and magnetic resonators," *Applied Physics Letters*, Vol. 90, No. 26, 263504, 2007.
3. Turpin, J. P., Q. Wu, D. H. Werner, B. Martin, M. Bray, and E. Lier, "Near-zero-index metamaterial lens combined with AMC metasurface for high-directivity low-profile antennas," *IEEE Trans. on Antennas and Propagat.*, Vol. 62, No. 1, 1928–1936, 2014.
4. Jiang, Z., Q. Wu, D. Brocker, P. Sieber, and D. Werner, "A low-profile high-gain substrate-integrated waveguide slot antenna enabled by an ultrathin anisotropic zero-index metamaterial coating," *IEEE Trans. on Antennas and Propagat.*, Vol. 62, No. 3, 1173–1183, 2014.
5. Aghanejad, I., H. Abiri, and A. Yahaghi, "Design of high-gain lens antenna by gradient-index metamaterials using transformation optics," *IEEE Trans. on Antennas and Propagat.*, Vol. 60, No. 9, 4074–4081, 2012.
6. Chen, X., H. F. Ma, X. Y. Zou, W. X. Jiang, and T. J. Cui, "Three-dimensional broadband and high-directivity lens antenna made of metamaterials," *Journal of Applied Physics*, Vol. 110, No. 4, 044904, 2011.
7. Yuan, L., W. Tang, H. Li, Q. Cheng, and T. Cui, "Three-dimensional anisotropic zero-index lenses," *IEEE Trans. on Antennas and Propagat.*, Vol. 62, No. 2, 4135–4142, 2013.
8. Ramaccia, D., F. Scattone, F. Bilotti, and A. Toscano, "Broadband compact horn antennas by using EPS-ENZ metamaterial lens," *IEEE Trans. on Antennas and Propagat.*, Vol. 61, No. 6, 2929–2937, 2013.
9. Lee, Y. J., J. Yeo, R. Mittra, and W. S. Park, "Application of electromagnetic bandgap (EBG) superstrates with controllable defects for a class of patch antennas as spatial angular filters," *IEEE Trans. on Antennas and Propagat.*, Vol. 53, No. 1, 224–235, 2005.
10. Zhou, B. and T. J. Cui, "Directivity enhancement to vivaldi antennas using compactly anisotropic zero-index metamaterials," *IEEE Antennas and Wireless Propagat. Lett.*, Vol. 10, 326–329, 2011.

11. Sun, M., Z. N. Chen, and X. Qing, "Gain enhancement of 60-GHz antipodal tapered slot antenna using zero-index metamaterial," *IEEE Trans. on Antennas and Propagat.*, Vol. 61, No. 4, 1741–1746, 2013.
12. Chen, L., Z. Lei, R. Yang, J. Fan, and X. Shi, "A broadband artificial material for gain enhancement of antipodal tapered slot antenna," *IEEE Trans. on Antennas and Propagat.*, Vol. 63, No. 1, 395–400, 2015.
13. Cao, W., B. Zhang, A. Liu, T. Yu, D. Guo, and Y. Wei, "Gain enhancement for broadband periodic endfire antenna by using split-ring resonator structures," *IEEE Trans. on Antennas and Propagat.*, Vol. 60, No. 7, 3513–3516, 2012.
14. Cao, W., B. Zhang, A. Liu, T. Yu, D. Guo, and Y. Wei, "Broadband high-gain periodic endfire antenna by using I-shaped resonator (ISR) structures," *IEEE Antennas Wireless Propag. Lett.*, Vol. 11, 1470–1473, 2012.
15. Wang, H., S.-F. Liu, L. Chen, W.-T. Li, and X.-W. Shi, "Gain enhancement for broadband vertical planar printed antenna with H-shaped resonator structures," *IEEE Trans. on Antennas and Propagat.*, Vol. 62, No. 8, 4411–4415, 2014.
16. Liu, R., Q. Cheng, J. Y. Chin, J. J. Mock, and T. J. Cui, "Broadband gradient index microwave quasi-optical elements based on non-resonant metamaterials," *Optics express*, Vol. 17, No. 23, 21030–21041, 2009.
17. Tang, W. X., H. Zhao, X. Zhou, J. Y. Chin, and T.-J. Cui, "Negative index material composed of meander line and SRRs," *Progress In Electromagnetics Research B*, Vol. 8, 103–114, 2008.
18. Qu, S.-W., J.-L. Li, Q. Xue, and C.-H. Chan, "Wideband periodic endfire antenna with bowtie dipoles," *IEEE Antennas Wireless Propag. Lett.*, Vol. 7, 314–317, 2008.
19. Smith, D., S. Schultz, P. Markos, and C. Soukoulis, "Determination of effective permittivity and permeability of metamaterials from reflection and transmission coefficients," *Physics Rev. B*, Vol. 65, No. 19, 195104, 2002.